Photodimerization-induced transition of helixes to vesicles based on coumarin-12-crown-4

Hui-Juan Wang [a], Heng-Yi Zhang [a], Wen-Wen Xing [a], Huang Wu [b], Yong-Liang Cui [a], Yu Liu [a],*

[a] *Department of Chemistry, State Key Laboratory of Elemento-Organic Chemistry, Nankai University, Tianjin 300071, China*
[b] *Department of Chemistry, Northwestern University, Evanston, IL 60208, United States*

ABSTRACT

Rational construction of fine-tuning and precisely controllable topological nanostructures based on supramolecular self-assembly system remains a challenge. Herein, coumarin-12-crown-4 (**1**) as a building block was synthesized by one-pot method and showed reversible high stereo-selective photodimerization (*anti*-head-to-head dimer (*anti*-HH-**1**): *syn*-head-to-head dimer (*syn*-HH-**1**) = 10.8:1) and photocleavage. Helical nanobelts were formed by the self-assembly of **1** through asymmetrical H-bonds, which were in concordance with the crystal state superstructure. Upon irradiation with 365 nm light, these nanobelts transformed into nanoballs which were constructed by three building blocks. Further, we investigated the photoreaction of **1** and got two pure covalent dimers (*anti*-HH-**1** and *syn*-HH-**1**). The *anti*-HH-**1** self-assembled into hollow micro-vesicles. The transformation of superstructures based on photo-controlled multiple blocks shines a light to the research on the relationship between molecules and superstructures.

© 2022 Published by Elsevier B.V. on behalf of Chinese Chemical Society and Institute of Materia Medica, Chinese Academy of Medical Sciences.

Tunable superstructures constructed by low-molecular weight building blocks have attracted considerable attention due to their wide range of applications in catalysis, biological functions, silica superstructures and so on [1–5]. The development of supramolecular chemistry provides an effective strategy for the construction of versatile superstructures which are responsive to various stimuli, such as light, temperature, pH, solvents and metal ions [6–11]. One general design strategy for the construction of stimuli-responsive superstructures is the introduction of photoresponsive building blocks such as azobenzene, vinylene, coumarin and diarylethene [12–15]. Coumarin as a weakly toxic dye can be extracted from many plants and plays an important role in the research of reversible photodimerization, biomaterials, electro-optical materials [16–21], but their potential application in the construction of superstructures has been rarely investigated. Aida *et al.* reported graphitic nanotubes with a photo stitching capability based on a novel coumarin-appended amphiphilic hexaperi-hexabenzocoronene [22]. Feng *et al.* constructed chiral nanoribbons which can curve and grow into higher ordered hollow microstructures by the co-assembly of chiral phenylalanine and achiral coumarin derivatives [23]. Zhang *et al.* reported macroscalar helices based on the co-assembly of temperature-responsive coumarin modified carbohydrate and 1,4-benzenediboronic acid [24]. On the other hand, crown ethers with hydrophilic ether oxygen chain and hydrophobic aromatic ring were always used to construct various superstructures with specific functions [25]. Fenniri *et al.* reported multichannel rosette nanotubes constructed by the entropically driven hierarchical self-assembly of cytosine modified crown ethers [26,27]. Shinkai *et al.* reported multilayered spherical, helical ribbon and tubular structures of silica with an application in metal-deposition for catalyst based on crown-appended cholesterol derivatives [4,28-30]. Nolte *et al.* tuned the chirality of helical fibers of phthalocyanine ring attached four crown ethers by adding K^+ ions [31]. Recently, we reported a snowflake-like clockwise helical assembly with photo-controlled chirality based on azobenzene bridged crown ether [32]. We also reported a nanosheet constructed by the assembly of sulfonated crown ether and diphenylalanine [33]. Here in, we synthesized a coumarin-12-crown-4 (**1**) with highly selective [2 + 2] cycloaddition of the coumarin groups to yield the *anti*-head-to-head dimer (*anti*-HH-**1**) and *syn*-head-to-head dimer (*syn*-HH-**1**) with a ratio of 10.8:1 (Fig. 1). Then we constructed a system with tunable superstructures based on the reversible photodimerization and photocleavage of **1** (Scheme 1). It is the first application of photo controlled multiple building blocks based on a coumarin derivative in the construction of tunable superstructures, to the best of our knowledge.

Brief synthetic route, compound characterization and assignment of protons for **1** are shown in Scheme S1 and Figs. S1-S3 (Supporting information). Single crystals of **1** were obtained by slow vapor diffusion of ethyl ether into the dichloromethane so-
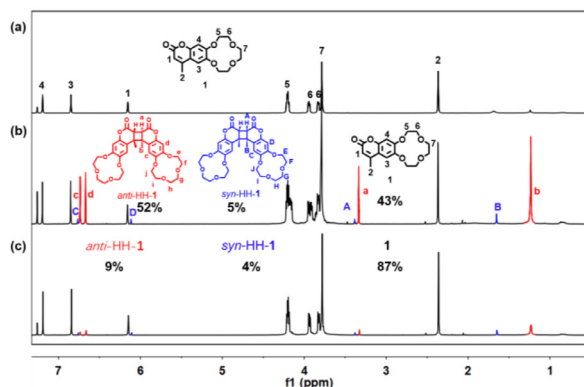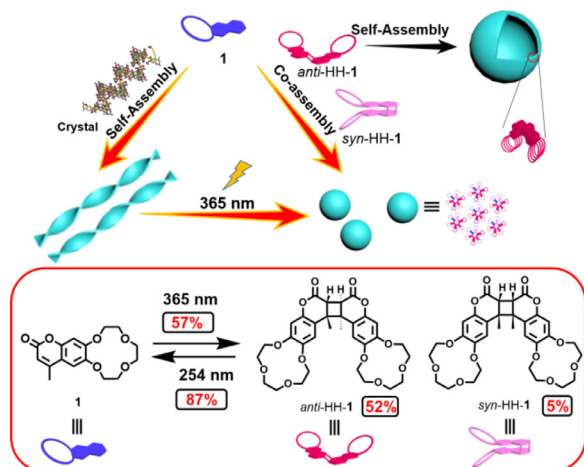
Fig. 1. ^{1}H NMR spectra (400 MHz, CDCl$_3$, 298 K) of **1** (a) before and (b) after light irradiation (365 nm, 2 × 6 W). (c) After irradiating the solution of (b) with 254 nm light (2 × 6 W).

Scheme 1. Schematic illustration and molecular structures of **1**, *anti*-HH-**1** and *syn*-HH-**1** as well as their crystal packing model or possible assembly mechanism.

Fig. 2. Absorption spectra of **1** upon irradiation at 365 nm for different time at 298 K ([**1**] = 10^{-4} mol/L) (a), **1**, *syn*-HH-**1** and *anti*-HH-**1** (b). Fluorescence spectra (λ_{ex} = 330 nm) of **1** upon irradiation at 365 nm for different time at 298 K ([**1**] = 5 × 10^{-5} mol/L) (c), **1**, *syn*-HH-**1** and *anti*-HH-**1** (d).

lution of **1**. The crystal structure of **1** was determined by single-crystal X-ray diffraction that revealed the coumarins adopt a head-to-head parallel arrangement. The distances between two adjacent C=C bonds are in the range from 3.63 Å to 3.76 Å, which are shorter than the favourable distance (4.7 Å) for the [2 + 2] dimerization (Fig. S17 in Supporting information) [34,35]. The well-preoriented coumarins not only favor dimerization of two adjacent **1** molecules, but also preferentially yield head-to-head dimers. Naturally, four cycloaddition isomers can be formed during the photodimerization process of coumarin as shown in Scheme S2 (Supporting information): *syn*-head-to head (*syn*-HH), *anti*-head-to-head (*anti*-HH), *syn*-head-to-tail (*syn*-HT), *anti*-head-to-tail (*anti*-HT) [36]. Considering these information, the photoreaction of **1** was characterized by ^{1}H NMR, UV–vis, fluorescence and ESI-MS. When a chloroform-*d* solution of **1** was irradiated by a lamp (365 nm, 2 × 6 W) in a quartz tube, a light yellow solution was obtained as the reaction proceeded. ^{1}H NMR spectra were first used to monitor the photoreaction process. With the increase of irradiation time, the peaks related to the protons (H$_1$, H$_2$, H$_3$ and H$_4$) of **1** decreased and two sets of upfield shifted peaks (H$_a$, H$_b$, H$_c$ and H$_d$; H$_A$, H$_B$, H$_C$ and H$_D$) appeared and increased gradually which were attributed to the [2 + 2] photodimerization of **1** (Fig. 1b and Scheme 1). The stereochemistry of the photoproducts was identified by either comparing the aromatic proton resonances (H$_c$, H$_d$, H$_C$ and H$_D$) [37] or the crystal structure of monomer. The almost identical ^{1}H NMR spectra which were measured after irradiation with 365 nm light for 8.5 h and 9 h respectively, indicated the pho-
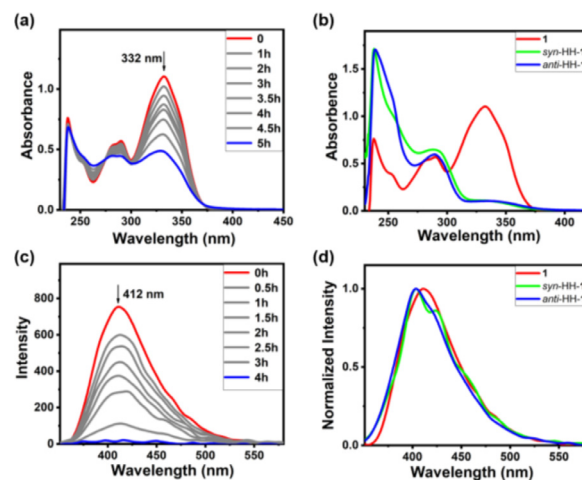
todimerization of **1** was complete after the irradiation of 8.5 h. According to the relative integrals of the protons, the ratio of **1**, *anti*-HH-**1** and *syn*-HH-**1** was calculated to be 43:52:5 in the photostationary state (PSS). Further irradiation with 254 nm light for 80 h, the ^{1}H NMR spectra indicated 87% conversion of the photoreaction products into **1** monomer (Fig. 1c). Electrospray ionization mass spectrometry (ESI-MS) provided further evidence for the formation of the intermolecular [2 + 2] cycloadduct (Fig. S4 in Supporting information, *m/z* 635.2103 for [(**1** dimer + Na$^+$)]$^+$). To further confirm the formation of *anti*-HH-**1** and *syn*-HH-**1**, we separated the photoproducts of **1** in chloroform and obtained three compounds (**1**, *anti*-HH-**1** and *syn*-HH-**1**). The photoreaction route, compound characterization and assignment of protons for *anti*-HH-**1** and *syn*-HH-**1** are shown in Scheme 1 and Figs. S5-S12 (Supporting information).

UV–vis absorption spectra and fluorescence spectra were also used to trace the photodimerization process of **1**. A chloroform solution of **1** was subjected to the irradiation with 365 nm light when the absorption and fluorescence were detected at 0.5 h or 1 h intervals (Figs. 2a and c). With the irradiation, the absorption peak of the coumarin monomer at 332 nm decreases gradually which means the formation of single bonds between cyclobutane (Fig. 2a) [34,38,39]. With the irradiation time increased from 0 to 5 h, the absorbance intensity at 332 nm decreased and achieved PSS. Further irradiation caused a collapse of the UV–vis curve due to the photobleaching. For fluorescence spectra, the emission at 412 nm decreased gradually until quenching with the increasing irradiation time of 365 nm light. As shown in Fig. 2b, the UV–vis spectrum of **1** showed two sharp peaks at 238 nm, 332 nm and one double peaks at 281 nm, 290 nm. The UV–vis spectra of *anti*-HH-**1** and *syn*-HH-**1** showed only two sharp peaks at 238 nm and 289 nm. Fig. 2d showed the fluorescence emission spectra of **1**, *anti*-HH-**1** and *syn*-HH-**1**. A strong fluorescence emission peak was detected at 413 nm in the chloroform solution of **1**. While both *anti*-HH-**1** and *syn*-HH-**1** show a slightly blue-shift peak at 411 nm and a shoulder peak at 434 nm only appeared in the spectrum of *syn*-HH-**1**. The fluorescence excitation spectra of **1**, *anti*-HH-**1** and *syn*-HH-**1** were shown in Fig. S14 (Supporting information), and the corresponding fluorescence quantum yields are 24.8%, 13.5% and 16.2%, respectively (Fig. S15 in Supporting information).

Further, we explored the morphological information of the photo-controlled building blocks based on **1**. Firstly, the morphologies of **1** were examined by scanning electron microscope (SEM)
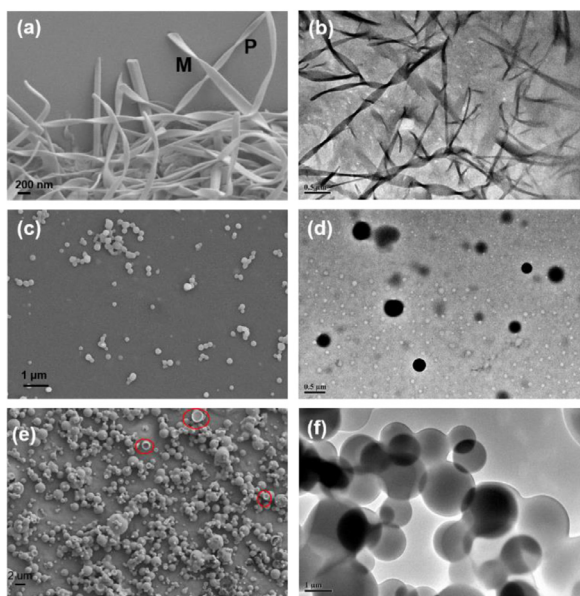
Fig. 3. (a) SEM and (b) TEM images of **1**; (c) SEM and (d) TEM images of **1** after irradiation with 365 nm light; (e) SEM and (f) TEM images of *anti*-HH-**1** (CH$_3$CN, 298 K).

Fig. 4. (a) Crystal structure of **1** in ball and stick model, (b) the unit cell of the single crystal of **1**, C–H···O 2.65(2) 2.60 2.66 2.71, (c) solid-state (super) structure of **1**.

and transmission electron microscopy (TEM) shown in Fig. 3 and Fig. S18 (Supporting information). A network composed of helical belts with one or two hundred nanometers wide, nanoscale thickness and microscale length (Figs. 3a and b). In the course of assembly, nanobelts with chiral P type mixed with few M types were constructed simultaneously (Fig. 3a). The above results indicate that there is asymmetric stacking during the period of self-assembly progress. Further, we explored the self-assembly behaviors of **1** in acetonitrile with different concentration. And found that the higher concentration of **1** lead to more helical belts (Fig. S18). The photo-controlled transformation of nanostructures was investigated by SEM and TEM images. The photodimerization of **1** leads to morphological variation from helical belts to nanoballs with diameter about hundreds of nanometers (Figs. 3c and d). It can be considered as the co-assembly of three building blocks (**1**, *anti*-HH-**1** and *syn*-HH-**1**). To further investigate the process, the TEM image of halftime irradiated solution of **1** was given in Fig. S13 and showed both helical nanobelts and nanoballs. We think the morphological changes from helixes to nanoballs were due to the transition from self-assembly of **1** to the co-assembly of the photoproducts. As displayed in Fig. S16 (Supporting information), the XRD spectra of **1**, photoproducts of **1** and *anti*-HH-**1** all showed sharp peaks, implying that the assemblies are ordered.

Since the self-assembly of achiral molecule **1** shows macroscopic helical property, it is essential to figure out the origin of chirality in nanobelts. Molecular structure and packing model of **1** were determined by single-crystal X-ray diffraction analysis. Single crystal superstructure, unit cell, and related crystal data of **1** are shown in Fig. 4 and Supporting information, respectively. Each molecule interacts with four neighboring ones through seven C–H···O interactions with distances ranging from 2.51 to 3.37 Å (Fig. 4b and Fig. S17 in Supporting information). In the solid-state superstructure, **1** assembles into a right-handed helix due to the intermolecular asymmetrical hydrogen bonds and π-π stacking. After the irradiation with 365 nm light, the photodimerization of **1** occurs accompanying with the formation of two new building blocks (*anti*-HH-**1** and *syn*-HH-**1**). Further to find out the possible molecular packing model after the irradiation with 365 nm light, we optimized molecular structures of *anti*-HH-**1** and *syn*-HH-**1** (Fig. S20 in Supporting information) by Gaussian 09 W. The two
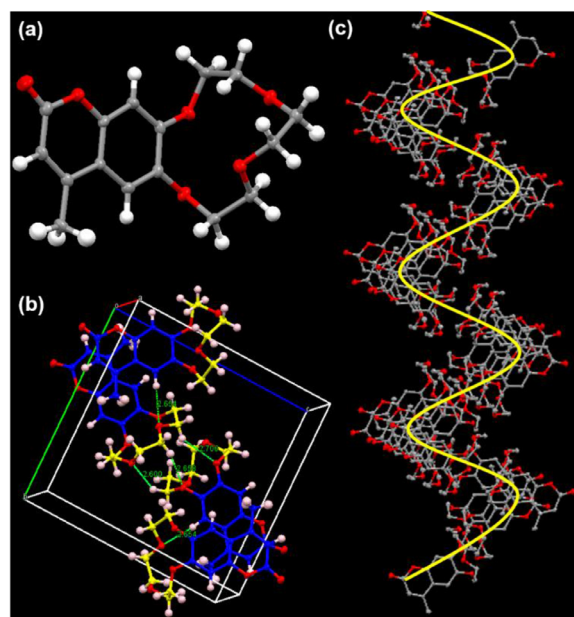
coumarins of *anti*-HH-**1** are not parallel to each other with a little skewing which may make a curve to the whole packing system of three building blocks. The coumarin groups of three building blocks folded by π-π stacking with ether oxygen chains outside. Due to the un-parallel aromatic ring of *anti*-HH-**1**, nanoballs with increased curvature compared to nanobelts were obtained. We have got the pure *anti*-HH-**1** through the photoreaction of **1** and purified by silica gel column chromatography. The self-assembly of *anti*-HH-**1** generated hollow balls with micrometers in diameter which were observed by TEM and SEM (Figs. 3e and f). A careful analysis of the SEM images which showed several ruptured microstructures (marked by red circle) and holes on the surface of these microstructures well illustrates the hollow interiors of balls (Fig. 3e and Fig. S19 in Supporting information) [40,41]. The possible molecular packing model of *anti*-HH-**1** was optimized and shown in Fig. S19c. The torison of coumarin after dimerization may caused the slight curvature which lead to a vesicle on the micron scale.

In summary, we designed and synthesized a coumarin derivative **1**, and found that **1** shows regio- and stereo-selected photodimerization to producing only head-to-head coumarin isomers (*anti*-HH-**1** and *syn*-HH-**1** with a ratio of 10.8:1) under the irradiation of 365 nm light due to the preorientation of the coumarins. And this coumarin derivative was utilized as photocontrolled reversible multiple building blocks with similar structures to construct photo-tunable superstructures which works like a game of 3D Tetris. The self-assembly of **1** formed a network consisted helical nanobelts which in accordance with the stacking model of single crystal of **1**. After the irradiation of 365 nm light, it turns to nanoballs as a result of the co-assembly of **1**, *syn*-HH-**1** and *anti*-HH-**1**. Further, we find the self-assembly of pure *anti*-HH-**1** form hollow micro-balls. This work explored the relationship between molecular structures and properties, provide new strategy for the construction of supramolecular functional materials.

Declaration of competing interest

The authors declare that they have no known competing financial interests or personal relationships that could have appeared to influence the work reported in this paper.

Acknowledgment

Supplementary materials

Supplementary material associated with this article can be found, in the online version, at doi:10.1016/j.cclet.2021.12.051.

References

[1] X. Dou, N. Mehwish, C. Zhao, et al., Acc. Chem. Rev. 53 (2020) 852–862.
[2] X. Zhou, H. Zhao, S. Liu, et al., Chin. Chem. Lett. 32 (2021) 761–764.
[3] P. Xing, Y. Zhao, Adv. Mater. 28 (2016) 7304–7339.
[4] J.H. Jung, Y. Ono, K. Sakurai, M. Sano, S. Shinkai, J. Am. Chem. Soc. 122 (2000) 8648–8653.
[5] L. Li, W. Tuo, Q. Zhu, et al., J. Am. Chem. Soc. 142 (2020) 20583–20587.
[6] S. Yagai, Y. Kitamoto, S. Datta, B. Adhikari, Acc. Chem. Res. 52 (2019) 1325–1335.
[7] L. Zhang, Y.M. Zhang, G.X. Liu, Y. Liu, Chin. Chem. Lett. 30 (2019) 120–122.
[8] P. Xing, Y. Li, Y. Wang, et al., Angew. Chem. Int. Ed. 57 (2018) 7774–7779.
[9] G. Yu, M. Xue, Z. Zhang, et al., J. Am. Chem. Soc. 134 (2012) 13248–13251.
[10] T. Zhang, Y.H. Liu, B.W. Hu, et al., Chin. Chem. Lett. 30 (2019) 949–952.
[11] G. Liu, J. Sheng, W.L. Teo, et al., J. Am. Chem. Soc. 140 (2018) 16275–16283.
[12] H.L. Sun, Y. Chen, X. Han, Y. Liu, Angew. Chem. Int. Ed. 56 (2017) 7062–7065.
[13] S. Yagai, M. Yamauchi, A. Kobayashi, et al., J. Am. Chem. Soc. 134 (2012) 18205–18208.
[14] M. Yamauchi, T. Ohba, T. Karatsu, S. Yagai, Nat. Commun. 6 (2015) 8936.
[15] J. Zhang, Q. Zou, H. Tian, Adv. Mater. 25 (2013) 378–399.
[16] H. He, M. Feng, Q. Chen, X. Zhang, H. Zhan, Angew. Chem. Int. Ed. 55 (2016) 936–940.
[17] Y. Cao, Y. Chen, Z. Zhang, et al., Chin. Chem. Lett. 32 (2021) 349–352.
[18] S.R. Trenor, A.R. Shultz, B.J. Love, E.T. Long, Chem. Soc. Rev. 104 (2004) 3059–3077.
[19] J.W. Chung, K. Lee, C. Neikirk, C.M. Nelson, Small 8 (2012) 1693–1700.
[20] P.P. Jia, L. Xu, Y.X. Hu, et al., J. Am. Chem. Soc. 143 (2021) 399–408.
[21] H. Yan, F. Huo, Y. Yue, J. Chao, C. Yin, J. Am. Chem. Soc. 143 (2021) 318–325.
[22] J. Motoyanagi, T. Fukushima, N. Ishii, T. Aida, J. Am. Chem. Soc. 128 (2006) 4220–4221.
[23] F. Wang, H. Qiu, C. Feng, Adv. Funct. Mater. 30 (2020) 2002936.
[24] S. Wang, M.C. Forster, K. Xue, et al., Angew. Chem. Int. Ed. 60 (2021) 9712–9718.
[25] J.H. Jung, H. Kobayashi, M. Masuda, T. Shimizu, S. Shinkai, J. Am. Chem. Soc. 123 (2001) 8785–8789.
[26] H. Fenniri, B.L. Deng, A.E. Ribbe, et al., Proc. Natl. Acad. Sci. U. S. A. 99 (2002) 6487–6492.
[27] H. Fenniri, B.L. Deng, A.E. Ribbe, J. Am. Chem. Soc. 124 (2002) 11064–11072.
[28] J.H. Jung, Y. Ono, K. Sakurai, M. Sano, S. Shinkai, J. Am. Chem. Soc. 122 (2000) 8648–8653.
[29] J.H. Jung, H. Kobayashi, M. Masuda, T. Shimizu, S. Shinkai, J. Am. Chem. Soc. 123 (2001) 8785–8789.
[30] J.H. Jung, Y. Ono, S. Shinkai, Langmuir 16 (2000) 1643–1649.
[31] H. Engelkamp, S. Middelbeek, R.J.M. Nolte, Science 284 (1999) 785–788.
[32] H.J. Wang, H.Y. Zhang, H. Wu, et al., Chem. Commun. 55 (2019) 4499–4502.
[33] W. Zhang, Y.M. Zhang, S.H. Li, et al., Angew. Chem. Int. Ed. 55 (2016) 11452–11456.
[34] P. Wei, H. Wang, K. Jie, F. Huang, Chem. Commun. 53 (2017) 1688–1691.
[35] G.M.J. Schmidt, Pure Appl. Chem. 27 (1971) 647–678.
[36] S.R. Trenor, A.R. Shultz, B.J. Love, T.E. Long, Chem. Rev. 104 (2004) 3059–3078.
[37] X. Yu, D. Scheller, O. Rademacher, T. Wolff, J. Org. Chem. 68 (2003) 7386–7399.
[38] J. Jiang, B. Qi, M. Lepage, Y. Zhao, Macromolecules 40 (2007) 790–792.
[39] N.K. Mal, M. Fujiwara, Y. Tanaka, Nature 421 (2003) 350–353.
[40] W. Ali, W. Gong, M. Hassan, et al., Chin. Chem. Lett. 32 (2021) 371–374.
[41] P.Y. Li, Y. Chen, Y. Liu, Chin. Chem. Lett. 30 (2019) 1190–1197.